Investigation of the effects of small fishing ports on the shoreline: a case study of Samsun, Turkey

Derya Ozturk[1] · Erdem Emin Maras[2]

Abstract

Shoreline change analysis is crucial for identifying coastal issues and understanding their underlying causes. This study focuses on investigating the coastal impacts of the Derekoy Fishing Port in Samsun, a city located on the Black Sea coast of Turkey. Temporal changes between 1984 and 2021 were analyzed using Landsat-5 TM/Landsat-8 OLI satellite images in conjunction with image processing and geographic information systems (GIS). Net shoreline movement (NSM), shoreline change envelope (SCE), end point rate (EPR), and linear regression rate (LRR) methods were used to investigate the changes in the shoreline. Polygon overlay analysis was utilized to determine the areas of erosion and accretion. The results indicate that prior to the port's construction, the coast remained relatively stable during the period of 1984–1995. However, sediment accretion occurred on the updrift side of the port, while erosion intensified on the downdrift side during the port's construction from 1995 to 2004. Despite the implementation of coastal protection structures to combat erosion, complete prevention was not achieved, and erosion shifted further eastward. Throughout 1984–2021, approximately 15.62 hectares of beaches were lost due to erosion, with a maximum value of -56.2 m recorded. The coastal erosion and the construction of coastal protection structures have disturbed coastal morphology and resulted in various environmental and socio-economic issues along the 19 Mayis and Atakum beaches. This study reveals the significant consequences of a small fishing port built without proper planning and adequate precautions, drawing attention to the problems.

Keywords Fishing port · Coastal erosion · Net shoreline movement · Shoreline change envelope · End point rate · Linear regression rate

Introduction

In its most basic definition, "shoreline" is a distinction/boundary between land and water (Dolan et al. 1980). Due to the dynamic nature of coasts, spatial changes occur in shorelines (Liu and Trinder 2018). Information about shoreline change is essential for analyzing erosion-accretion trends, assessing coastal disasters, designing coastal infrastructure, and protecting the coastal environment (Boak and Turner 2005; Liu and Trinder 2018). The shoreline can naturally change continuously due to sea-level rise, tidal effects, and seasonal changes in waves and winds (Kudale 2010).

However, natural factors alone cannot account for all the significant shoreline changes. Anthropogenic effects also cause considerable changes in the shoreline (Gonçalves et al. 2019). Human-induced coastal erosion in Europe exceeds coastal erosion caused by natural factors (Rijn 2011; Tsoukala et al. 2015). The main anthropogenic factors causing shoreline change include a decrease in sediment carried to the coast due to river regulation and dam construction (Ozturk and Sesli 2015; Bergillos et al. 2016), the construction of ports, marinas (Tsoukala et al. 2015), and hard coastal defense/protection structures (Ozturk et al. 2015), offshore dredging (Chu et al. 2015) and near-shore vegetation clearing (Singh et al. 2021). Investigating anthropogenic impacts in coastal areas is crucial for developing policies and plans for coastal protection and sustainability (Gonçalves et al. 2019).

Large/medium/small ports and fishing ports comprise various coastal structures, including breakwaters, jetties, groins, and reclamation bunds (Kudale 2010). The

✉ Derya Ozturk
  dozturk@omu.edu.tr

1 Department of Geomatics Engineering, Ondokuz Mayis University, 55139 Samsun, Turkey

2 Department of Flight Training, Vocational School of Civil Aviation, Samsun University, 55080 Samsun, Turkey

construction of coastal structures involves intervention in the coastal processes of a region (Deepika et al. 2014). Since coastal structures affect local wave conditions, hydrodynamic processes, currents, sediment transport, and sand movement, they can cause significant changes to the adjacent coast (Kudale 2010). Coastal structures built along the coast pose a serious threat of beach erosion on sandy beaches while causing a significant increase in waves on rocky shores. This effect is more pronounced in coastal areas with high longshore currents compared to other coasts. In these regions, sediment accretion on the updrift side and erosion on the downdrift side are inevitable (Kudale 2010; Tsoukala et al. 2015). Beach erosion can even lead to the complete destruction of beaches (Tsoukala et al. 2015).

Due to the lack of knowledge regarding coastal structures and disruptions in costing processes, the behavior of the applied system may not meet expectations, and coastal projects may produce undesirable results on the coast (Kudale 2010; Görmüş et al. 2014). For instance, the construction of ports, aimed at improving tourism and/or the local economy, can result in various adverse environmental, ecological, and socio-economic effects (Tsoukala et al. 2015). Port construction may cause sediment accretion on the updrift side and erosion on the downdrift side, adversely affecting coastal processes. Adverse effects can even begin during the construction phases of port development (Kudale 2010). The ecological impacts of port construction are not limited solely to the adjacent coastal areas but also extend further into the surrounding regions, gradually affecting the coastal ecosystems on a regional scale (OSPAR Commission 2009). Major ecological impacts include the loss of coastal habitats, reduction in biological productivity and biodiversity, and disruption of ecological balance (Dugan et al. 2011; Tsoukala et al. 2015). Coastal erosion also has significant socio-economic effects, adversely affecting recreation, tourism, settlements, and infrastructure (Özhan 2002). Damage to the beaches, buildings, and infrastructure caused by the increase in the frequency of sea floods following the decrease in the beach's width, falling of trees, and degradation of coastal agricultural lands cause deterioration of the aesthetics of the coastal landscape (Prasetya 2006; Pollard et al. 2019). Consequently, this situation negatively impacts tourism and causes a loss of value in real estate in the coastal area and an increase in regional investment risks (Tsoukala et al. 2015; Hoang Thi Thu et al. 2022). Tsoukala et al. (2015) state that coastal protection structures aimed at preventing erosion rarely solve the problem, and in some cases, withdrawing the port is the best solution.

It is necessary to monitor the shoreline changes to manage the complex effects of the ports. Monitoring shoreline changes enables the understanding of the interaction between ports and the adjacent coasts, the detection of coastal erosion and/or coastal flooding, the determination

of the amount of change, and the identification of underlying causes of the problem (Tsoukala et al. 2015). Potential data sources for investigating the spatio-temporal characteristics of the shoreline include maps, land surveying with in situ geolocation systems, aerial photographs, and digital satellite imagery (Liu and Trinder 2018; Martínez et al. 2022). Data selection depends on factors such as cost, time, data resolution, and data availability for specific dates (Atkinson 2001; Boak and Turner 2005). Digital satellite images obtained through remote sensing offer several advantages, including detailed spectral information, quick acquisition, and cost-effectiveness (Kavurmacı et al. 2013; Bhatti and Tripathi 2014; Suresh and Jain 2018). Furthermore, shoreline extraction can be performed using semi-automatic/automatic methods, and spatial shoreline change analysis can be easily and accurately conducted using Geographic Information Systems (GIS) (Deepika et al. 2014).

Determining the shoreline position comprises two stages. The first step is to select and define a shoreline indicator feature. In the second stage, the shoreline is determined from the data based on the selected shoreline indicator (McAllister et al. 2022). The shoreline, conventionally defined as the boundary where water and land surfaces intersect, exhibits dynamic characteristics and is subject to various data-related challenges. Consequently, the concept of a shoreline indicator has emerged to address these complexities. A shoreline indicator refers to a discernible feature utilized as a substitute to approximate the precise position of the shoreline (Boak and Turner 2005).Three approaches are commonly used as shoreline indicators. The first approach uses coastal features that can be visually distinguished from true/false color images as shoreline indicators. The high water line (HWL) is often utilized for this purpose. However, accurately extracting shorelines using this method relies on clearly distinguishing the shoreline from the image (Pajak and Leatherman 2002). In some cases, the HWL may appear as a transition zone instead of a distinct line, or it may not be visible at all. The slow drying of sand after previous waves can obscure the wet/dry boundary. Therefore, determining the shoreline based on the HWL is subjective and can cause uncertainty and inconsistency (Liu and Trinder 2018). The second approach considers the mean high water line (MHWL), determined by intersecting tidal data with the shore profile. However, this approach requires 3D profile data (McAllister et al. 2022). In the third approach, the shoreline determined through image processing techniques is accepted as the shoreline indicator (Boak and Turner 2005; Liu and Trinder 2018). Particularly for images with medium or low spatial resolution, the use of semi-automatic/automatic shoreline determination through digital image processing techniques yields more accurate results, as visually determining the shoreline from the image becomes challenging (Liu and Trinder 2018). To determine the shoreline

from satellite images using digital image processing techniques, various methods are employed, including image classification, filtering, single-band or multi-band density slicing, and spectral indices (Ouma and Tateishi 2006; Ghorai and Mahapatra 2020). Spectral indices are widely used due to their ease of implementation and the ability to integrate different spectral indices (Ozturk et al. 2015; Sunder et al. 2017; Toure et al. 2019).

Shoreline change analysis is based on calculating the total amount of change within a specified period and the rate of change (monthly/yearly) from a series of shorelines (Burningham and Fernandez-Nunez 2020; Dereli and Tercan 2020). When conducting temporal comparisons of shoreline changes, utilizing a single shoreline indicator is crucial to ensure consistency (Liu and Trinder 2018). Multi-temporal data are necessary to determine temporal changes in the shoreline. However, the availability of high-resolution satellite images is limited to the period after 2000, making them unsuitable for studying long-term change detection. On the other hand, low spatial resolution poses a significant challenge in determining shoreline changes from satellite images over long historical intervals (Li et al. 2015). Consequently, due to the difficulty of simultaneously providing high spatial resolution and extended temporal coverage in remote sensing, the choice of shoreline change period and data should be based on the characteristics of the study area (Atkinson 2001). The Landsat program, dating back to 1972, provides freely available archive data with a 16-day revisit period starting from Landsat-4 (Liu and Trinder 2018). This offers valuable opportunities to identify changes over long periods, making it highly applicable in various fields (Yu et al. 2011; Choung and Jo 2016; Daud et al. 2021).

Samsun, located in the Black Sea Region of Turkey, is a city that has achieved significant development in various aspects, including education, health, transportation, industry, trade, and the economy. It is also the most populous city in the region. Samsun attracts many tourists during summer due to its appealing features, strategic location, well-established transportation infrastructure, beautiful beaches, and tourism facilities. The districts of Atakum and 19 Mayis, in particular, have long been significant contributors to domestic tourism and the daily lives of the city's residents. However, the construction of the Derekoy Fishing Port in the 19 Mayis district, aimed at meeting the growing fishing demands of the region, has resulted in significant coastal deterioration. While the western part of the port experienced sediment accretion, severe erosion occurred in the eastern part, affecting approximately 50% of the Atakum coast. Although several studies (Bakkaloğlu 2006; Yüksek 2008; Candemir and Özdemir 2010; Güner 2019) have highlighted the adverse conditions caused by the erosion in this region, to our knowledge, no study quantitatively addressed the coastal changes until now. Despite the fragile nature of the

area, there is a lack of information regarding the spatio-temporal variation of erosion and sediment accretion, the factors influencing these dynamics, and the environmental consequences of shoreline changes. Therefore, conducting a quantitative analysis of shoreline changes and investigating the cause-and-effect relationships will make a valuable contribution toward understanding the current state of the coasts and determining the areas at risk of erosion more accurately.

This study aims to quantitatively assess the shoreline change and beach erosion caused by the Derekoy Fishing Port. It also seeks to highlight the reasons behind these changes and the potential negative consequences if preventive measures are not implemented. In order to achieve this, we conducted an investigation of the approximately 19.5 km long coast encompassing the Derekoy Fishing Port using remote sensing and GIS techniques. The analysis covered the period between 1984 and 2021, utilizing shorelines derived from Landsat-5 TM/Landsat-8 OLI satellite images through the integration of normalized difference water index (NDWI) and modified normalized difference water index (MNDWI). Shoreline changes were determined using net shoreline movement (NSM) and shoreline change envelope (SCE), while annual shoreline change rates were calculated using end point rate (EPR) and linear regression rate (LRR). Additionally, spatio-temporal areal changes were evaluated through polygon overlay analysis.

Study area

The city of Samsun, located on the Black Sea coast of Turkey, has a population of approximately 1.4 million as of 2021 (TSI 2021). It is the most populous and developed city among the 18 provinces in the Black Sea region, owing to its geographical and socio-economic characteristics (Samsun Chamber of Commerce and Industry 2017). The coastal areas of Samsun along the Black Sea consist of low-lying beaches with low coastal indentation, primarily due to the presence of coastal plains formed by the Yesilirmak and Kizilirmak deltas. The climate in Samsun is mild, with hot summers and warm, rainy winters in the coastal regions (TMEUCC 2012). The average temperature during the hottest four-month period between June and September is 21.8 °C, with an average sunshine duration of 7.9 h (TGDM 2022).

Samsun's coastal areas are renowned for their sandy beaches and favorable climate, making them a popular tourist destination for both city residents and neighboring provinces. The districts of Atakum and 19 Mayis are particularly sought after by tourists due to their extensive beaches, coastal promenades, and recreational amenities (TMEUCC 2012). The shoreline lengths of these districts are approximately 20.8 km and 19.6 km, respectively. However, these

coasts have undergone significant deterioration, especially in the past 50 years, due to the pressures of urbanization, population growth, and socio-economic developments (Ozturk 2017). This degradation has negatively impacted the potential for sea and coastal tourism.

Samsun holds a significant position in the Black Sea region regarding its fishing potential, and the growing demand for fishing in the area and the country has led to the construction of fishing ports (TMEUCC 2012). In 2021, out of the 385 fishing ports in Turkey, Samsun is home to five fishing ports (TMAF 2022). The Derekoy Fishing Port, with a main breakwater length of 1010 m and a secondary breakwater of 370 m, was constructed in the 19 Mayis district between 1995 and 2004 (Akpınar 2019).

After the construction of the Derekoy Fishing Port, the adjacent beaches experienced coastal erosion, resulting in the uprooting and toppling of trees and the reduction

in the width of sandy beaches. To mitigate erosion, various coastal protection structures such as groins and offshore breakwaters were implemented. In 2001–2002, seven T-shaped groins were constructed along the 1.5 km stretch of the coast. However, despite these efforts, erosion continued to escalate following the lengthening of the main breakwater of the Derekoy Fishing Port in 2003. As a response, offshore breakwaters were subsequently constructed. Offshore breakwaters of two (8, 9) in 2004, two (10, 11) in 2006, five (12–16) in 2010, four (17–20) in 2011, one (21) in 2004–2006, five (22–26) in 2013, two (27, 28) in 2014, five (29–33) in 2015, and three (38–40) in 2018 were built. In addition to that, I-shaped (straight) groins of three (34–36) in 2017 and one (37) in 2018 were constructed. As of 2018, a total of 40 coastal protection structures have been established along the 7 km coast (Fig. 1).
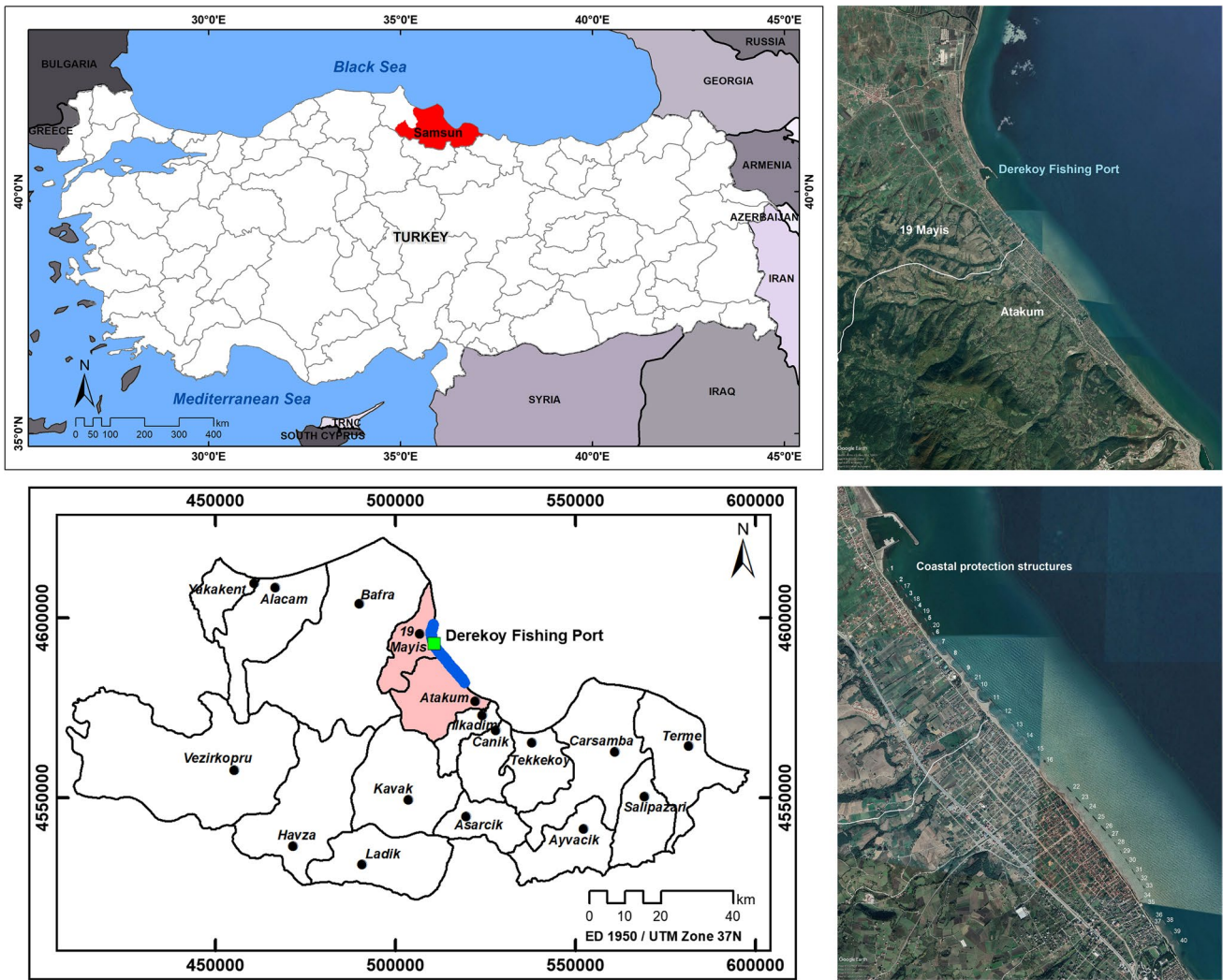

Fig. 1 Location of the study area: The 19 Mayis district, where the Dereköy fishing port was built, and the neighboring Atakum district

The research was conducted within a specific geographical area that spans a 19.5 km stretch along the Samsun coast. Within this area, 13.8 km extends eastward from the main breakwater of the Derekoy Fishing Port, comprising 3.2 km in the 19 Mayis district and 10.6 km in the Atakum district. The remaining 5.7 km runs westward in the 19 Mayis district. The location of the study area can be found in Fig. 1.

Data and methods

In this study, we examined shoreline changes over a 37-year period from 1984 to 2021 using Landsat Collection 2 Level-2 satellite images (Path/Row: 175/31) obtained freely from the USGS Earth Explorer data portal (USGS 2022a). The USGS performed geometric and atmospheric corrections on the satellite data, and the Committee on Earth Observation Satellites (CEOS) approved the Level-2 products as analysis-ready data for land (USGS 2022b). The satellite data were in the UTM projection/WGS 84 datum. Rectification involved resampling using Cubic Convolution. For atmospheric corrections, the Landsat Ecosystem Disturbance Adaptive Processing System (LEDAPS) (Claverie et al. 2015) was used for Landsat-5 TM images, and the Land Surface Reflectance Code (LaSRC) (Vermote et al. 2016) was used for Landsat-8 OLI images. The multispectral bands of Landsat-5 TM/Landsat-8 OLI satellite images have a pixel size of 30 m (USGS 2022c).

We considered the construction dates of the Derekoy Fishing Port and the coastal protection structures to select the dates of the satellite images. Accordingly, Landsat-5 TM images were used for before the construction of the port (1984), the start and end date of the construction of the port (1995, 2004), and 2011, while Landsat-8 OLI images were used for 2021. To minimize the impact of seasonal variations on the analysis results, we chose images from months that were in close proximity to each other (Table 1).

Shorelines were extracted from satellite images using image processing techniques and converted to vector format. The shoreline change analysis encompassed various periods, including 1984–1995, 1995–2004, 2004–2011, 2011–2021, 1984–2004, 2004–2021, and 1984–2021. High-resolution free images for 2011 and 2021 from GE Pro were used to verify the shorelines extracted from Landsat images (Table 1). GE Pro, developed by Google Inc., is a virtual

globe program that provides access to geo-referenced satellite (e.g., Quickbird, Worldview, Ikonos) or aerial images with spatial resolutions finer than 1 m in numerous regions worldwide (Scollar and Palmer 2008; Qi and Wang 2014; Luo et al. 2019). The most critical limitation of GE Pro images is that getting the original multispectral band data is impossible. It means getting actual pixel brightness values is not possible, so we cannot perform information extraction using image processing techniques. However, the high spatial resolution allows for on-screen digitization through visual interpretation (Tilahun and Teferie 2015; Malarvizhi et al. 2016). Therefore, for the accuracy assessment, we extracted the shorelines for 2011 and 2021 from the high-resolution images using visual interpretation and on-screen digitizing and compared the amount of change from Landsat images for the 2011–2021 period with the results from GE Pro images.

The extraction of shorelines from Landsat images and subsequent analyses of shoreline changes were conducted using ArcGIS 10.0 software (ESRI, Redlands, CA), while the digitization of GE Pro images was performed using GE Pro. The flowchart outlining the primary steps involved in shoreline extraction and determination of changes is presented in Fig. 2. In the initial stage, shorelines were extracted from Landsat-5 TM images captured in 1984, 1995, 2004, and 2011, as well as from Landsat-8 OLI images obtained in 2021, through the integration of NDWI and MNDWI indices. Subsequently, in the second stage, the extent of shoreline change was evaluated using the NSM and SCE techniques, while shoreline change rates were computed using EPR and LRR methodologies. Additionally, the analysis included the assessment of areal changes through polygon overlay analysis. Lastly, an accuracy assessment was performed by utilizing GE Pro images.

Extraction of shorelines

Due to the limited spatial resolution of Landsat-5 TM/Landsat-8 OLI satellite images, it is not possible to distinguish shorelines visually. Consequently, we employed digital image processing techniques using a third-group shoreline indicator to extract shorelines from the images. Specifically, we utilized the NDWI (McFeeters 1996) and MNDWI (Xu 2006) indices (Eqs. 1 and 2). To convert the images into binary form, we assigned a value of 1 to land and 0 to water,

Table 1 Data used in the analysis

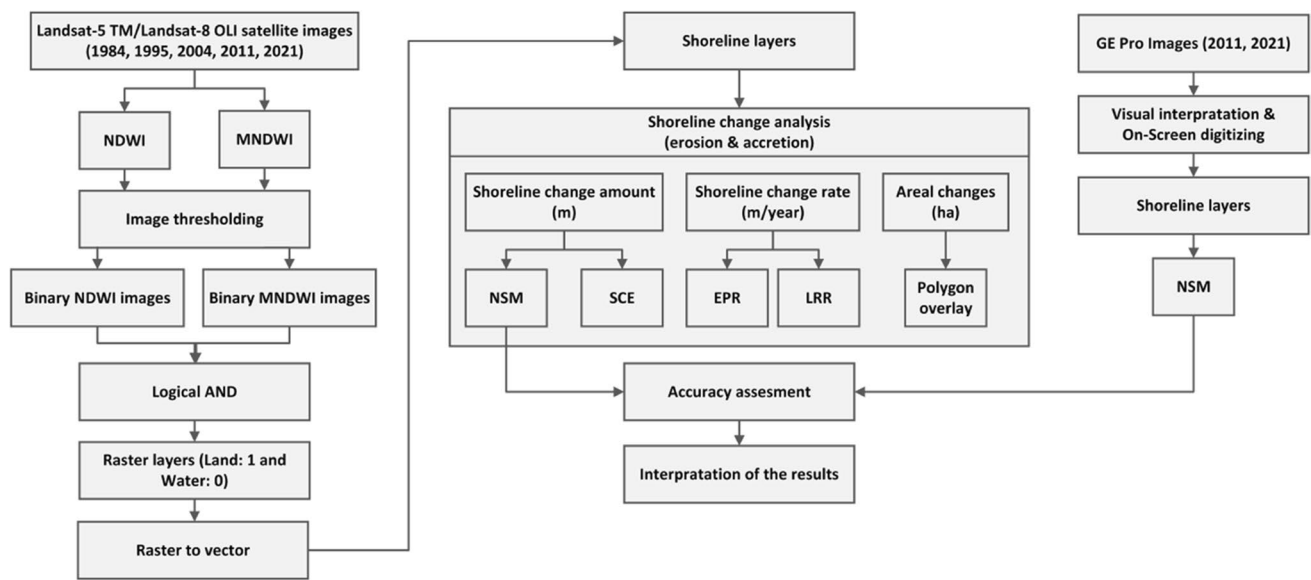| Analysis	Data and dates
Analysis of shoreline changes in the 1984–2021 period	Landsat-5 TM satellite images of 1984.08.12, 1995.10.14, 2004.09.20, 2011.09.08, and Landsat-8 OLI of 2021.10.21
Confirmation of shoreline change	GE Pro images of 2011.09.21 and 2021.03.28

Fig. 2 Workflow scheme for shoreline extraction and determination of change

based on a threshold value determined using known pixels in the NDWI and MNDWI images. The final image was generated by integrating the NDWI and MNDWI indices by multiplying the binary images using the "logical AND operator." The final image had a pixel size of 30 m, based on the pixel size of the Landsat-5 TM/Landsat-8 OLI satellite images. We then converted the raster data into vector form and transferred it to the database. Figure 3 illustrates the steps involved in shoreline extraction for 2021.

$$NDWI = (Green - NIR)/(Green + NIR) \qquad (1)$$

$$MNDWI = (Green - MIR)/(Green + MIR) \qquad (2)$$

In Eqs. 1 and 2, Green represents the reflectance value in the green band, NIR represents the reflectance value in the near-infrared band, and MIR represents the reflectance value in the mid-infrared band.

Determination of shoreline change

Since shoreline change exhibits different characteristics in various regions of the study area, the area was examined by dividing it into three zones. Zone 1 comprises the west side of the Derekoy Fishing Port. Zone 2 encompasses the eastern side of the port, where erosion is severe, and coastal protection structures are located. Zone 3 is located east of Zone 2 and experiences relatively less erosion. To conduct the analysis, baselines were initially created approximately 1 km parallel to the shorelines in the seaward direction, aligning with the general curvature of all shorelines. Then we created transects on the baselines at 50 m intervals. Analyses were

performed using 118 transects (transects 1–118) for Zone 1, 155 (Transects 119–273) for Zone 2, and 120 (Transects 274–393) for Zone 3 (Fig. 4).

We used the NSM and SCE methods to determine the amount of shoreline change, and the EPR and LRR methods to calculate the annual rate of change between 1984 and 2021. The shorelines based on the same shoreline indicator were used to ensure consistency in determining temporal changes in the shorelines. In this context, shorelines obtained using the water indices from Landsat-5 TM/Landsat-8 OLI satellite images of 1984, 1995, 2004, 2011, and 2021 were used as input data in the analyses.

According to the NSM method, the difference between the distances of the oldest and most recent shoreline to the baseline is calculated for each transect in determining the shoreline change (Eq. 3) (Wiles et al. 2022). The (-) sign shows erosion, while the (+) sign shows accretion (Ozturk and Sesli 2015).

$$NSM = \begin{cases} (d_{oldest} - d_{youngest}) & \textit{If the baseline is on the water side} \\ -(d_{oldest} - d_{youngest}) & \textit{If the baseline is on the land side} \end{cases}$$

$$(3)$$

where d_{oldest} represents the distance of the oldest shoreline to the baseline, and $d_{youngest}$ represents the distance of the youngest shoreline to the baseline.

In determining the shoreline change using the SCE method, the maximum changes that occur independently of the dates are taken into account. For each transect, the distance between the nearest and farthest shorelines to the baseline is determined (Eq. 4) (Weerasingha and Ratnayake 2022). If the baseline is on the water side, erosion is indicated by a negative sign (-) when the farthest shoreline
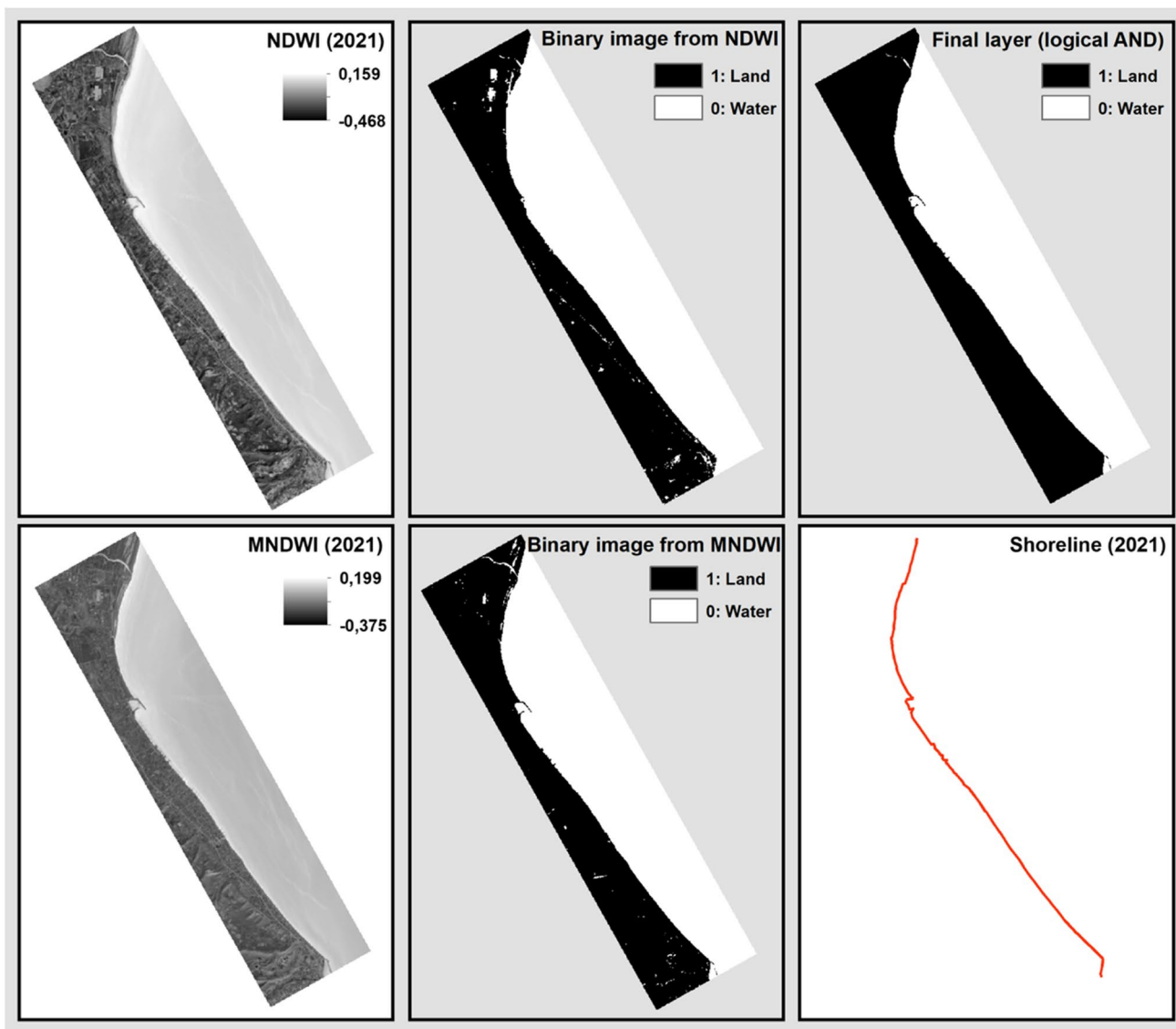
Fig. 3 Extraction of shoreline from NDWI and NDWI indices for 2021

distance is more recent, and accretion is indicated by a positive sign (+) when it is older. Conversely, if the baseline is on the land side, accretion is indicated by a positive sign (+) when the farthest shoreline distance is more recent, and erosion is indicated by a negative sign (-) when it is older (Ozturk and Sesli 2015).

$$SCE = \begin{cases} \left(d_{farthest} - d_{nearest}\right) \textit{If the baseline is on the water side and the } d_{farthest} \textit{ is} \\ \textit{older;If the baseline is on the land side and the } d_{farthest} \textit{ is more recent} \\ -\left(d_{farthest} - d_{nearest}\right) \textit{If the baseline is on the water side and the } d_{farthest} \textit{ is} \\ \textit{more recent; If the baseline is on the land side and the } d_{farthest} \textit{ is older} \end{cases} \tag{4}$$

where $d_{farthest}$ represents the distance of the farthest shoreline to the baseline, and $d_{nearest}$ represents the distance of the nearest shoreline to the baseline.

In calculating the shoreline change rate using EPR, the amount of change in each transect for the two specified dates is divided by the time interval, and rates of change can be calculated as erosion (-) and accretion (+) (Eq. 5). If the annual shorelines are used, and the distance is in meters, the results are in m/year (Das et al. 2021; Wiles et al. 2022). When more than two shorelines are available, the rates of
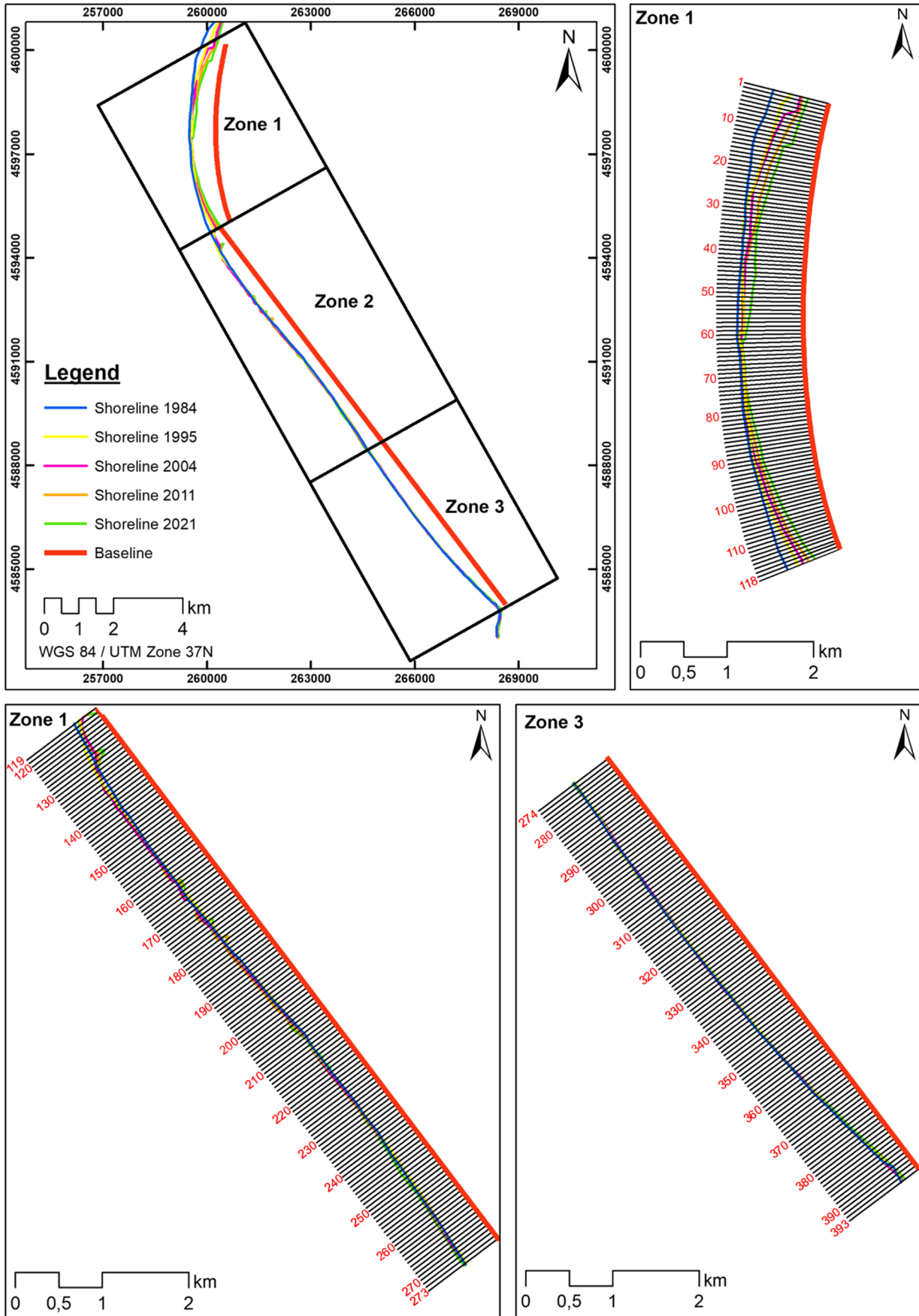
◀**Fig. 4** Division of the study area into zones and creation of transects for shoreline change analysis

change can be calculated using two selected dates (Ozturk et al. 2015).

$$EPR = \begin{cases} \frac{(d_{old} - d_{young})}{\Delta t} & \textit{If the baseline is on the water side} \\ -\frac{(d_{old} - d_{young})}{\Delta t} & \textit{If the baseline is on the land side} \end{cases} \tag{5}$$

where d_{old} represents the distance of the older shoreline to the baseline, d_{young} represents the distance of the younger shoreline to the baseline, and Δt represents the time interval between the two specified dates.

In calculating the shoreline change rate using the LRR based on the least squares method, the most appropriate linear regression line for each transect is determined by considering shorelines for all dates included in the analysis (Eq. 6) (Sowmya et al. 2019; Weerasingha and Ratnayake 2022).

$$y = mx + b \tag{6}$$

where m represents the slope of the line, b denotes the constant value, x signifies the independent variable, and y represents the dependent variable. In this study, the independent variable corresponds to the years of the shorelines, while the dependent variable pertains to the distances from the baseline to the shorelines for each transect (Das et al. 2021; Elfadaly et al. 2022). The rate of change of the shoreline is equal to "-m" if the baseline is on the water side and "m" if it is on the land side.

To evaluate the predictive accuracy of the linear regression model for shoreline changes along each transect, the coefficient of determination (R^2) is calculated (Eq. 7) (Barrett 1974; Nandi et al. 2016). R^2 provides information regarding the goodness of fit of the model and serves as a measure of uncertainty (Maiti and Bhattacharya 2009; Kumar et al. 2010). R^2 ranges from 1.0 to 0.0, with values closer to 1.0 indicating that the regression line explains a significant portion of the variation in the dependent variable, while values closer to 0.0 indicate that the line explains only a small portion of the variation in the dependent variable (Himmelstoss et al. 2018). In this study, $R^2 > 0.8$ was chosen as the threshold of certainty for calculating the shoreline change rate, following Maiti and Bhattacharya (2009) and Kumar et al. (2010).

$$R^2 = 1 - \frac{\sum \left(y_{measure} - y_{predict}\right)^2}{\sum \left(y_{measure} - y_{mean}\right)^2} \tag{7}$$

where $y_{measure}$ represents the measured distance from the baseline for a shoreline data point, $y_{predict}$ represents the predicted distance from baseline based on the regression equation, and y_{mean} represents the mean of the measured shoreline distances from the baseline.

Determination of areal changes

We performed polygon overlay analysis for each zone to determine the areal losses and gains caused by shoreline changes between 1984 and 2021 (Fig. 5). Overlay analysis involves the superimposition of layers based on Boolean algebra rules to generate new information (Piovan 2020). The polygons for the three zones in the study area were created by combining the zone boundaries with the shorelines from the dates chosen for change determination. The land was coded as 1, and water was coded as 0 in the polygon layers. The amounts of erosion and accretion (in hectares) between 1984 and 2021 were calculated using the overlay analysis following Boolean rules (Ozturk and Sesli 2015), as shown in Table 2.

Accuracy assessment

The accuracy assessment of the shoreline changes obtained from Landsat images was conducted by comparing the shoreline changes determined using the NSM method from Landsat and GE Pro images for the period of 2011–2021. The shorelines from high-resolution images in 2011 and 2021, accessed through GE Pro, were determined through visual interpretation using the HWL shoreline indicator. Visual interpretation involves the on-screen digitizing of objects based on visual image interpretation elements such as tone, texture, size, shape, pattern, and association (Kusimi and Dika 2012; Arveti et al. 2016; Svatonova 2016). The differences and correlation coefficients between the change values determined using the NSM method from Landsat and GE Pro for the period 2011–2021 were calculated. Differences lower than one pixel are considered reliable for long-term studies (Coca and Ricaurte-Villota 2022). Following the correlation scale suggested by Evans (1996), 0.00–0.19 is considered very weak, 0.20–0.39 is weak, 0.40–0.59 is moderate, 0.60–0.79 is strong, and 0.80–1.00 is very strong correlation.

Results

Based on the analysis conducted across 393 transects within the study area, various shoreline change parameters were determined, including the amount of shoreline change (m), annual change rates (m/year), erosion amounts (m and m/year), and areal changes (ha). These calculations were performed for the entire study area as well as for each zone. In the interpretation of the analysis results, negative (-) values indicate erosion (backward in the direction of land), while
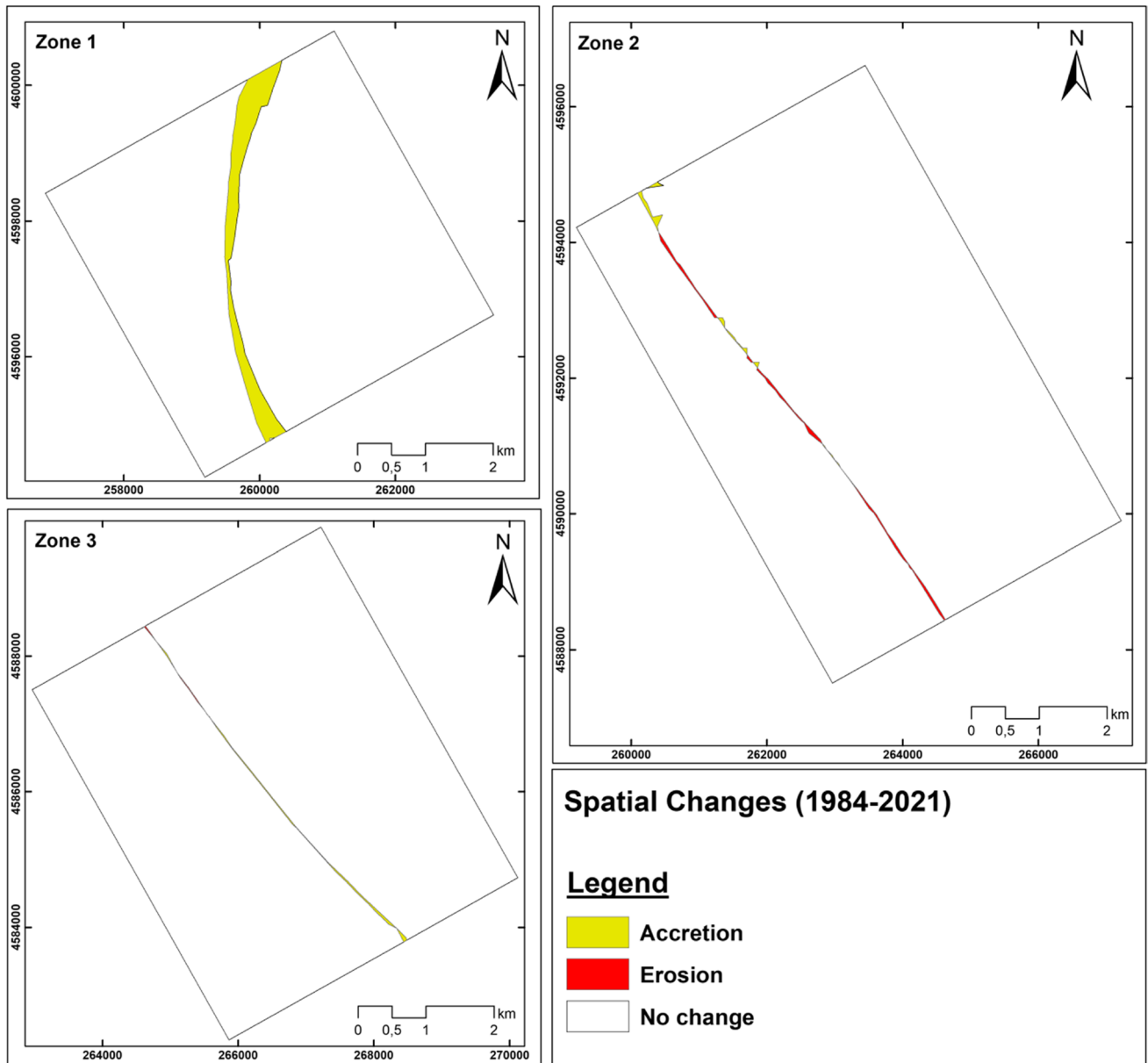
Fig. 5 Determination of spatio-temporal areal changes using overlay analysis in three zones

positive (+) values indicate accretion (forward in the direction of the sea).

Table 2 Boolean interpretation for the evaluation of the coastal change

Old layer	Young layer	Final layer
1	1	No change
1	0	Erosion
0	1	Accretion
0	0	No change

Shoreline change

We calculated the amounts of shoreline change using the NSM and SCE methods. Table 3 presents a summary of the statistical information regarding shoreline changes for various periods, including 1984–1995, 1995–2004, 2004–2011, 2011–2021, 1984–2004, 2004–2021, and 1984–2021. The 1984–1995 period represents the changes observed before the construction of the Derekoy Fishing Port, while the 1995–2004 period reflects the changes resulting from the port's construction. The 2004–2011 period corresponds to the effects of the initial 16 coastal protection structures, and the 2011–2021 period captures

Table 3 Shoreline change amount (m) determined using the NSM method (1984–1995, 1995–2004, 2004–2011, 2011–2021, 1984–2004, 2004–2021, and 1984–2021)

NSM (m)								
Zone		1984–1995	1995–2004	2004–2011	2011–2021	1984–2004	2004–2021	1984–2021
Zone 1 (118 transects)	min	−18.7	−20.7	−51.0	−3.5	14.7	20.5	42.2
	max	208.5	193.1	121.8	142.5	332.3	239.0	440.7
	mean	65.2	29.8	40.0	62.8	95.1	102.7	197.8
Zone 2 (155 transects)	min	−51.9	−51.6	−32.8	−53.2	−67.3	−51.7	−56.2
	max	81.5	99.5	52.4	102.2	119.0	125.0	196.0
	mean	0.6	−10.6	−2.5	2.3	−10.0	−0.2	−10.2
Zone 3 (120 transects)	min	−12.5	−24.3	−15.1	−17.2	−34.7	−19.5	−18.0
	max	19.5	13.0	18.4	58.9	19.2	43.8	58.3
	mean	5.2	−2.1	2.1	5.3	3.2	7.4	10.6

the impacts of an additional 24 coastal protection structures. We attempted to determine the changes that occurred until the completion of the port construction using the 1984–2004 period, the changes that occurred after the port construction using the 2004–2021 period (considering the combined effects of the port and coastal protection structures), and the total shoreline change using the 1984–2021 period.

According to the NSM results in Table 3, in terms of mean values, accretion in Zone 1 and Zone 3 and erosion in Zone 2 were observed in the 1984–2021 period. In Zone 2, the mean change was 0.6 m in the 1984–1995 period (before the port construction) and −10.6 m in 1995–2004 (during the construction of the port). The mean change, which was −2.5 m in the 2004–2011 period due to the construction of the first 16 coastal protection structures, is 2.3 m in the 2011–2021 period when additional coastal structures were built. The change in the 1984–2021 period is −10.2 m. −10.0 m of this change occurred during the completion of the port construction, and the -0.2 m shows the change after the construction of the coastal protection structures. The mean change over the 1984–2021 period is 197.8 m in Zone 1 and 10.6 m in Zone 3.

All shorelines in the 1984–2021 period (1984, 1995, 2004, 2011, and 2021) were considered in determining the shoreline changes using the SCE method. Table 4 provides a summary of the statistical information regarding the changes obtained using the SCE method, which calculates the distances between the nearest and farthest shorelines to the baseline in each transect.

According to Table 4, the mean changes in the 1984–2021 period, considering the combined effect of 1984, 1995, 2004, 2011, and 2021 using the SCE method, are 198.3 m for Zone 1, −18.4 m for Zone 2, and 13.0 m for Zone 3. Regarding minimum values, the landward retreat reaches −84.2 m in Zone 2 and −33.4 m in Zone 3. In Zone 1, the shoreline has moved towards the sea, ranging from 43.0 m to 440.7 m.

Table 4 Shoreline change amount (m) determined using the SCE method (1984–2021)

SCE (m)		
Zone		1984–2021 (Years: 1984, 1995, 2004, 2011, 2021)
Zone 1 (118 transects)	min	43.0
	max	440.7
	mean	198.3
Zone 2 (155 transects)	min	−84.2
	max	211.6
	mean	−18.4
Zone 3 (120 transects)	min	−33.4
	max	58.9
	mean	13.0

To determine the annual shoreline change rates (m/year), we employed the EPR and LRR methods. Table 5 provides the summary statistics of the EPR results for the 1984–1995, 1995–2004, 2004–2011, 2011–2021, 1984–2004, 2004–2021, and 1984–2021 periods. Additionally, Table 6 presents the LRR results for the 1984–2021 period (considering all the years: 1984, 1995, 2004, 2011, and 2021).

According to the annual change rates calculated using the EPR method (Table 5), the highest mean change is −1.2 m/year in Zone 2 in the 1995–2004 period covering the port construction process, 6.3 m/year in Zone 1 in the 2011–2021 period, and 0.5 m/year in Zone 3 in 1984–1995 and 2011–2021 periods. The mean annual rate of change for the entire 1984–2021 period is 5.3 m/year for Zone 1, −0.3 m/year for Zone 2, and 0.3 m/year for Zone 3.

According to Table 6, the mean annual rate of change during the 1984–2021 period is 5.2 m/year for Zone 1, −0.4 m/year for Zone 2, and 0.2 m/year for Zone 3, considering the combined effect of the years 1984, 1995, 2004, 2011, and 2021, using the LRR method. Regarding minimum values,

Table 5 Shoreline change rate (m/year) using the EPR method (1984–1995, 1995–2004, 2004–2011, 2011–2021, 1984–2004, 2004–2021, and 1984–2021)

EPR (m/year)								
Zone		1984–1995	1995–2004	2004–2011	2011–2021	1984–2004	2004–2021	1984–2021
Zone 1 (118 transects)	*min*	−1.7	−2.3	−7.3	−0.3	0.7	1.2	1.1
	max	19.0	21.5	17.4	14.2	16.6	14.1	11.9
	mean	5.9	3.3	5.7	6.3	4.8	6.0	5.3
Zone 2 (155 transects)	*min*	−4.7	−5.7	−4.7	−5.3	−3.4	−3.0	−1.5
	max	7.4	11.1	7.5	10.2	6.0	7.4	5.3
	mean	0.1	−1.2	−0.4	0.2	−0.5	0.0	−0.3
Zone 3 (120 transects)	*min*	−1.1	−2.7	−2.2	−1.7	−1.7	−1.1	−0.5
	max	1.8	1.4	2.6	5.9	1.0	2.6	1.6
	mean	0.5	−0.2	0.3	0.5	0.2	0.4	0.3

Table 6 Shoreline change rate (m/year) using the LRR method (1984–2021)

LRR (m/year)		
Zone		1984–2021 (Years: 1984, 1995, 2004, 2011, 2021)
Zone 1 (118 transects)	*min*	1.0
	max	11.5
	mean	5.2
	Number of transects with $R^2 > 0.8$	89 (75%)
Zone 2 (155 transects)	*min*	−1.6
	max	4.8
	mean	−0.4
	Number of transects with $R^2 > 0.8$	12 (8%)
Zone 3 (120 transects)	*min*	−0.6
	max	1.3
	mean	0.2
	Number of transects with $R^2 > 0.8$	10 (8%)

the rate of landward retreat reaches −1.6 m/year in Zone 2 and −0.6 m/year in Zone 3. In Zone 1, the shoreline has moved toward the sea, with an annual rate of change ranging from 1.0 m/year to 11.5 m/year. Out of the total transects analyzed, 89 in Zone 1, 12 in Zone 2, and 10 in Zone 3 have shoreline change rates above the 0.8 threshold of certainty suggested by Maiti and Bhattacharya (2009) and Kumar et al. (2010). Values below 0.8 indicate uncertainties in the measurement of the shoreline change rate. These uncertainties were mainly observed in transects adjacent to the port and coastal protection structures.

Determination of erosion

The total number of transects and the total erosion amounts/yearly erosion rates determined by the NSM, SCE, EPR, and LRR methods are presented in Table 7.

Table 7 demonstrates that the period with the highest number of eroded transects is 1995–2004, with 232 transects according to the NSM and EPR methods. According to the EPR method, the annual rate is −368.5 m/year in total, and the total change for the whole period is −3316.4 m. According to the EPR method, the highest erosion rate in terms of minimum values was −7.3 m/year in the 2004–2011 period.

For the 1984–2021 period, the NSM method calculated a mean erosion of −22.7 m across 138 transects, resulting in a total erosion of −3128.2 m. On the other hand, the SCE method calculated a total erosion of −5244.7 m with a mean erosion of -36.9 m across 142 transects. When considering annual rates for the 1984–2021 period, the EPR method determined erosion in 138 transects with a mean erosion rate of −0.6 m/year and total erosion of -84.5 m/year. Additionally, the LRR method identified erosion in 147 transects, with a mean erosion rate of −0.7 m/year and total erosion of -95.9 m.

Table 7 Amount and rate of erosion

Period	Change amount (m)				Change rate (m/year)			
	Number of transects	Total	Mean	Min	Number of transects	Total	Mean	Min
	NSM				EPR			
1984–1995	93	−1195.4	−12.9	−51.9	93	−108.7	−1.2	−4.7
1995–2004	232	−3316.4	−14.3	−51.6	232	−368.5	−1.6	−5.7
2004–2011	148	−1785.4	−12.1	−51.0	148	−255.1	−1.7	−7.3
2011–2021	117	−1885.0	−16.1	−53.2	117	−188.5	−1.6	−5.3
1984–2004	145	−2525.4	−17.4	−67.3	145	−126.3	−0.9	−3.4
2004–2021	129	−2154.2	−16.7	−51.7	129	−126.7	−1.0	−3.0
1984–2021	138	−3128.2	−22.7	−56.2	138	−84.5	−0.6	−1.5
	SCE				LRR			
1984–2021 (1984, 1995, 2004, 2011, 2021)	142	−5244.7	−36.9	−84.2	147	−95.9	−0.7	−1.6

The distribution of erosion is presented in Table 8, revealing that Zone 2 experiences the highest erosion in all periods. The number of transects in Zone 2 increased from 58 in 1984–1995 to 132 in 1995–2004, and subsequently decreased to 91 in 2004–2011 and 61 in 2011–2021.

According to the EPR values, Zone 2 has an annual mean erosion rate of −2.0 m/year in the 1995–2004 period, with a total value of −258.2 m/year across all transects. In the same period, the NSM method indicates a mean erosion of −17.6 m and a total erosion of −2323.7 m for all transects

Table 8 Amount and rate of erosion by zones

Period	Zone	Number of transects	Total NSM	Mean NSM	Min NSM	Number of transects	Total EPR	Mean EPR	Min EPR
1984–1995	1	6	−62.4	−10.4	−18.7	6	−5.7	−0.9	−1.7
	2	58	−988.1	−17.0	−51.9	58	−89.8	−1.5	−4.7
	3	29	−144.8	−5.0	−12.5	29	−13.2	−0.5	−1.1
1995–2004	1	31	−381.4	−12.3	−20.7	31	−42.4	−1.4	−2.3
	2	132	−2323.7	−17.6	−51.6	132	−258.2	−2.0	−5.7
	3	69	−611.3	−8.9	−24.3	69	−67.9	−1.0	−2.7
2004–2011	1	18	−311.1	−17.3	−51.0	18	−44.4	−2.5	−7.3
	2	91	−1266.2	−13.9	−32.8	91	−180.9	−2.0	−4.7
	3	39	−208.0	−5.3	−15.1	39	−29.7	−0.8	−2.2
2011–2021	1	1	−3.5	−3.5	−3.5	1	−0.3	−0.3	−0.3
	2	61	−1534.8	−25.2	−53.2	61	−153.5	−2.5	−5.3
	3	55	−346.7	−6.3	−17.2	55	−34.7	−0.6	−1.7
1984–2004	1	0	–	–	–	0	–	–	–
	2	119	−2363.5	−19.9	−67.3	119	−118.2	−1.0	−3.4
	3	26	−161.9	−6.2	−34.7	26	−8.1	−0.3	−1.7
2004–2021	1	0	–	–	–	0	–	–	–
	2	89	−1764.8	−19.8	−51.7	89	−103.8	−1.2	−3.0
	3	40	−389.4	−9.7	−19.5	40	−22.9	−0.6	−1.1
1984–2021	1	0	–	–	–	0	–	–	–
	2	117	−2926.4	−25.0	−56.2	117	−79.1	−0.7	−1.5
	3	21	−201.9	−9.6	−18.0	21	−5.5	−0.3	−0.5
		Number of transects	Total SCE	Mean SCE	Min SCE	Number of transects	Total LRR	Mean LRR	Min LRR
1984–2021 (1984, 1995, 2004, 2011, 2021)	1	0	–	–	–	0	–	–	–
	2	122	−4898.7	−40.2	−84.2	127	−91.4	−0.7	−1.6
	3	20	−346.0	−17.3	−33.4	20	−4.4	−0.2	−0.6

in Zone 2. Moving on to Zone 3, the number of transects increased from 29 in 1984–1995 to 69 in 1995–2004, decreased to 39 in 2004–2011, and then increased again to 55 in 2011–2022. In Zone 1, erosion was observed in 6 transects in 1984–1995, 31 transects in 1995–2004, 18 transects in 2004–2011, and 1 transect in 2011–2021. For the 1984–2021 period, the NSM method identified erosion in 0, 117, and 21 transects for Zones 1, 2, and 3, respectively, while the SCE method identified erosion in 0, 122, and 20 transects in the same order. The mean erosion rates using the EPR method were −0.7 m/year for Zone 2 and -0.3 m/year for Zone 3 in the 1984–2021 period. Using the LRR method, the mean erosion rates were −0.7 m/year for Zone 2 and −0.2 m/year for Zone 3.

Areal changes

The amounts of erosion and accretion (in hectares) determined for the 1984–2021 period through overlay analysis are presented in Table 9. In Zone 1, a total accretion of 107.97 ha is observed as a single continuous piece. Zone 2 has a total accretion of 6.55 ha spread across seven areas, while 14.60 ha of erosion occurred in six areas. For Zone 3, accretion amounting to 7.40 ha is observed in four areas, whereas 1.02 ha of erosion was determined in four areas.

Accuracy assessment

We compared the amount of shoreline change from the Landsat data with the change from the GE Pro high-resolution images in the 2011–2021 period to evaluate the accuracy of the shorelines for the Landsat data. Table 10 compares the shoreline change amounts determined using the NSM method for the three zones in the study area.

There is a difference of 6.1 m in Zone 1, −1.9 m in Zone 2, and 4.7 m in Zone 3 in terms of the mean values of shoreline changes determined using the NSM method for the period 2011–2021. The differences between the mean

Table 9 Areal changes in the 1984–2021 period

Zone		Erosion (ha)	Accretion (ha)
Zone 1	*min*	–	107.97
	max	–	107.97
	total	–	107.97
Zone 2	*min*	0.01	0.0
	max	5.97	3.42
	total	14.60	6.55
Zone 3	*min*	0.01	0.01
	max	0.68	6.17
	total	1.02	7.40
Whole area	*total*	15.62	13.95

Table 10 Comparison of the shoreline change amounts determined using the NSM method (2011–2021)

Zone		NSM (m)-GE Pro	NSM (m)-Landsat	Difference (GE Pro-Landsat) (m)
Zone 1	*min*	0.0	−3.5	3.5
	max	137.1	142.5	−5.4
	mean	68.9	62.8	6.1
Zone 2	*min*	−74.4	−53.2	−21.2
	max	86.6	102.2	−15.6
	mean	0.4	2.3	−1.9
Zone 3	*min*	−11.1	−17.2	6.1
	max	29.4	58.9	−29.5
	mean	10.0	5.3	4.7

values were less than 0.3 pixels. The obtained results were considered acceptable because sub-pixel precision was provided, as stated in Coca and Ricaurte-Villota (2022). Pearson correlation values were calculated to determine the relationship between the amount of changes in the shoreline determined from Landsat and GE Pro images, resulting in 0.733 for Zone 1, 0.859 for Zone 2, and 0.640 for Zone 3. According to the Evans scale (Evans 1996), Zone 1 and Zone 3 have a strong correlation, while Zone 2 has a very strong correlation.

Discussion

Urban development, industrial activities, energy terminals, shipyards, secondary housing, tourism, recreation, maritime trade, maritime transport, and fishing all vie for space along the coasts, which have been significant areas of social, economic, and cultural interaction throughout history. These pressures contribute to an increase in unplanned development, leading to various societal, economic, and environmental challenges such as coastal destruction, degradation of the natural environment and ecological balance, and pollution (TMEUCC 2022).

This study focuses on investigating the shoreline changes caused by the construction of a small fishing port and its associated environmental effects. The preservation of the 19 Mayis and Atakum beaches is crucial for tourism and the local economy, as these areas attract visitors from Samsun and neighboring provinces for recreational activities and swimming. The Samsun Integrated Coastal Areas Management and Planning Project-Spatial Strategy Plan (TMEUCC 2012) emphasizes the importance of utilizing the sea and coastal facilities more efficiently while preserving the natural beach quality of the Atakum district. The plan also encourages the development of recreational activities such as sea and water sports, and camping, particularly

considering the presence of 19 Mayis University within the area. However, following the construction of the Derekoy Fishing Port, which is the subject of this study, the balance of the sea-coastal ecosystem has deteriorated. The port has disrupted wave movements in the sea over time, preventing the transportation of sand from west to east. As a result, severe coastal erosion has occurred on the beach adjacent to the east of the port breakwater (Bakkaloğlu 2006; Yüksek 2008; Candemir and Özdemir 2010; Güner 2019). Our study includes various analyses to assess the extent of shoreline change and erosion.

We analyzed the amount and annual rate of change, as well as the total areal changes, to investigate the changes between 1984 and 2021. The amount of shoreline change (m) was determined using the NSM method for the period between 1984 and 2021. Additionally, the maximum change

during that period, considering the years 1984, 1995, 2004, 2011, and 2021, was determined using the SCE method. The annual shoreline change rates (m/year) were calculated as the net annual rate of change between 1984 and 2021 using the EPR method, and the annual rate of change was determined using the LRR method, considering five different dates in 1984, 1995, 2004, 2011, and 2021. Figure 6a presents a comparison of the amount of change using the SCE and NSM methods, while Fig. 6b compares the annual rate of change using the EPR and LRR methods. Additionally, correlation values were calculated to compare the methods, revealing a correlation of 0.968 between NSM and SCE, and a correlation of 0.983 between EPR and LRR. The results obtained from the SCE and NSM methods were consistent for the 1984–2021 period, indicating that the overall change observed aligns with the changes observed during
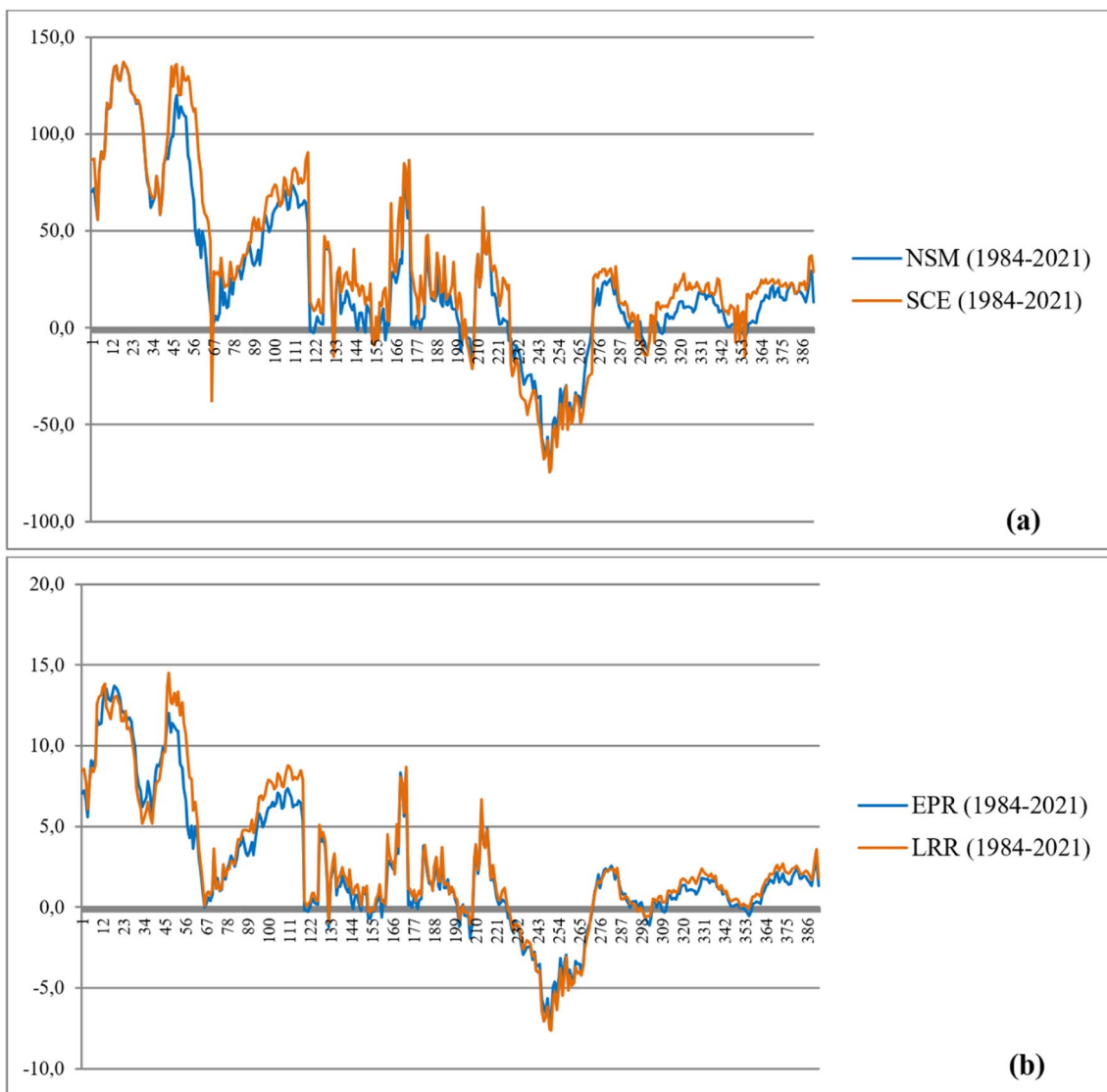

Fig. 6 Comparison of method results for amount and rate of changes. **a** Comparison of NSM and SCE (**b**) Comparison of EPR and LRR

the intervening years. Similarly, the results obtained from the EPR and LRR methods showed a high level of similarity.

Using the NSM method, it was observed that the effects of change had different trends in the three zones of the study area (Table 3). In Zone 1, which is the left side of the port breakwater, the mean value of shoreline change exhibited distinct variations. It measured 29.8 m in the 1995–2004 period, increased to 40.0 m in the 2004–2011 period, and further rose to 62.8 m in the 2011–2021 period. Notably, an apparent accretion effect was observed in this region.

In Zone 2, during the 1995–2004 period, the minimum value was −51.6 m (maximum erosion), with a mean change of −10.6 m. In the 2004–2011 period, the minimum value was −32.8 m (maximum erosion), with a mean change of −2.5 m. In the 2011–2021 period, the maximum erosion reached −53.2 m, with a mean change of 2.3 m. Evaluating the mean values in Zone 2, it was evident that the erosion effect observed during the 1995–2004 period decreased during the construction of coastal protection structures, but did not completely disappear. Notably, when comparing the maximum erosion values (minimum values), the highest value occurred during the 2011–2021 period.

In Zone 3, erosion was less than in Zone 2 in terms of mean value during the 1995–2004 period. In the periods 2004–2011 and 2011–2021, although the erosion situation seems to favor Zone 3 in terms of mean values, the presence of maximum erosion up to −17.2 m demonstrates the severity of the situation that persists. Examining the changes over the longest period (1984–2021), the mean change values were 197.8 m for Zone 1, −10.2 m for Zone 2, and 10.6 m for Zone 3. In terms of the maximum changes in this period using the SCE method, mean values were 198.3 m in Zone 1, −18.4 m in Zone 2, and 13.0 m in Zone 3 (Table 4). Consequently, the total change in Zone 1 during the 1984–2021 period was relatively close to the maximum changes observed. However, in Zone 2 and Zone 3, the maximum change exceeded the total change. This difference, particularly noticeable in Zone 2, indicated a partial decrease in erosion due to the construction of coastal protection structures after 2001. Regarding the annual rate of change calculated using the EPR method for different periods, the greatest change occurred with 6.3 m in Zone 1, 0.5 m in Zone 3 during the periods of 1984–1995 and 2011–2021, and −1.2 m in Zone 2 during the 1995–2004 period (Table 5). Analyzing the annual rate of change for the 1984–2021 period, a 0.1 m difference was observed for all three zones between the EPR results (representing the annual rate of total change) and the LRR results (indicating the general trend based on all shorelines) (Table 6). These findings demonstrated that the absolute rate of change between 1984 and 2021 in all zones generally aligned with the overall change trend. Nevertheless, the shoreline changes were found to be more unstable in the transects near the Dereköy

Fishing Port and the coastal protection structures that were constructed gradually between 2001 and 2018. This instability was manifested in the LRR analysis with the uncertainty in the sections close to the port and coastal protection structures, aligning with findings reported by Maiti and Bhattacharya (2009) and Kumar et al. (2010).

When focusing specifically on the eroded transects, Zone 2 had 132 transects, Zone 3 had 69 transects, and Zone 1 had 31 transects during the highest erosion period (1995–2004). According to the NSM and EPR methods, there were a total of 232 eroded transects out of the 393 transects analyzed in the study area (Table 8). In this period, the highest annual mean erosion rate was observed in Zone 2 with −2.0 m, while the second-highest rate was −1.4 m in Zone 1, which had the fewest transects. For Zone 3, this value was −1.0 m. Zone 2 is the region where the most erosion occurs in all periods.

When evaluating the absolute effect during the 1984–2021 period, no erosion was observed in Zone 1. In Zone 2, erosion occurred in 117 transects with an annual rate of −1.5 m/year, while in Zone 3, erosion was observed in 21 transects with an annual rate of −0.5 m/year (Table 8). The results obtained from the LRR method for the same period indicated erosion in 127 transects. Therefore, we conclude that the absolute effect determined by the EPR method is consistent with the general trend determined by the LRR method.

The areal changes determined by the overlay analysis show a gain of 107.97 ha in Zone 1, a loss of 14.60 ha and a gain of 6.55 ha in Zone 2, and a loss of 1.02 ha and a gain of 7.40 ha in Zone 3 for the period of 1984–2021. Zone 1 did not experience any loss in this period, while Zone 2 had a net loss of 8.05 ha. In Zone 3, there was both accretion and erosion. Overall, a total of 15.62 ha of beach area was lost due to erosion in the study area (Table 9).

According to these evaluations, the coastal protection structures built to prevent the erosion that occurred following the construction of the Dereköy Fishing Port could not wholly prevent the erosion but only shifted the erosion toward the east. As a result, the coastal areas did not attain a stable state. The construction of the port in the 19 Mayıs district has also significantly impacted the neighboring district of Atakum, which is a prominent area in Samsun known for domestic tourism, with its coast and natural beaches. The shoreline stretching approximately 9 km eastward from the port breakwater has been affected by coastal erosion, resulting in very limited beach areas (Fig. 7). Coastal erosion has caused the beach to nearly disappear in several locations. Figure 8 illustrates the substantial changes that have occurred between 2011 and 2022.

Coastal protection structures have been partially effective in preventing erosion, but they have also led to the degradation of the natural coastal structure and a decline

in aesthetics. In some areas, sand has accumulated between these structures, creating artificial filling areas (Fig. 9a). Over time, offshore breakwaters have merged with the coast, forming tombolo-like formations (Fig. 9b). The absence of water circulation between the coastal protection structures has caused the proliferation of excessive algae and

pollution (Fig. 9c). This has resulted in unpleasant odors and discomfort for the surrounding communities. Additionally, the placement of rocks/stones for coastal protection (rock/stone-filled coastal fortifications) along the shoreline has further contributed to the deterioration of the natural structure (Fig. 9d). The falling trees, damage to buildings,
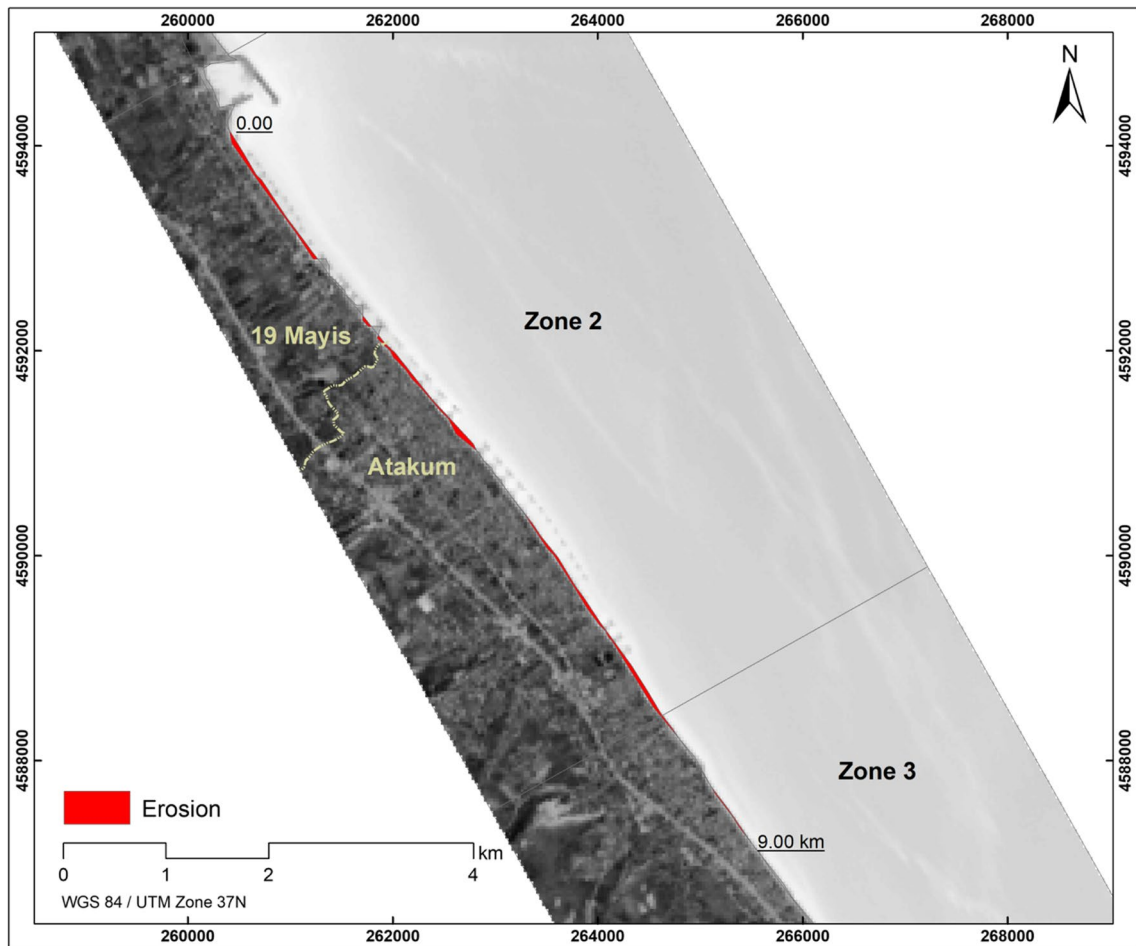
Fig. 7 Coastal erosion in 19 Mayis and Atakum

Fig. 8 Loss of the beach due to coastal erosion in the Atakum district (GE Pro 7.3.4.8642)
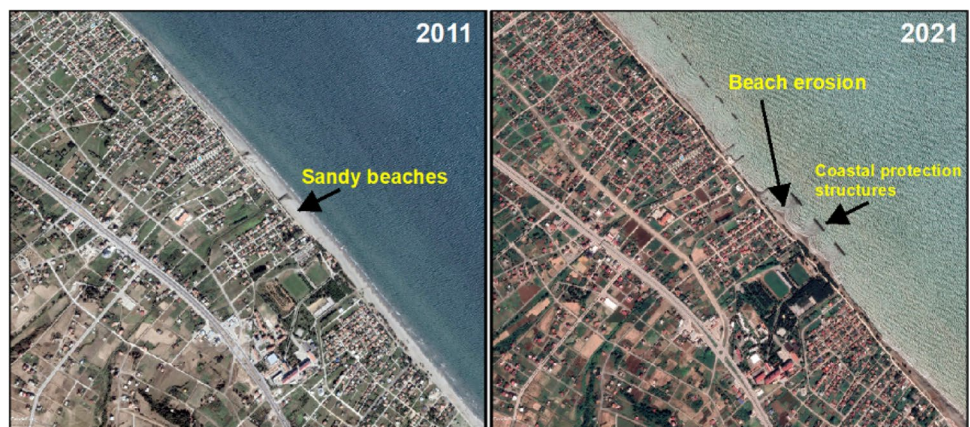
Fig. 9 Environmental impacts of coastal protection structures. **a** Filling areas formed by the accumulation of sand between the groins (GE Pro 7.3.4.8642, September 17, 2019). **b** Tombolo-like formations resulting from the merging of offshore breakwaters with the coast (GE Pro 7.3.4.8642, September 17, 2019). **c** Presence of algae and pollution between coastal protection structures (June 11, 2020). **d** Coastal fortification with rock/stone fill laid along the seaside (March 27, 2021)

and infrastructure have incurred additional costs, while the decline in coastal aesthetics has negatively impacted tourism and real estate values, leading to socio-economic losses (Yüksek 2008; Güner 2019).

In this study, we found similar findings to Kudale (2010), Tsoukala et al. (2015), and Gonçalves et al. (2019) regarding the adverse effects of port construction on coasts with sandy beaches. The construction of ports on the shores of Samsun with sandy beaches inevitably caused erosion. Due to the lack of preliminary research, accurate planning, and initial measures (Bakkaloğlu 2006), a series of coastal protection structures had to be built. However, with each additional coastal protection structure, the erosion was shifted further east, resulting in a deterioration of the coastal form. In some cases, the utilization of rock/stone fortifications as a cost-effective and immediate protective measure has resulted in the formation of artificial shores. As a result, the coastal protection structures and arrangements implemented to address erosion have had a negative impact on the environment, tourism, and the economy.

The most significant limitation of this study pertained to data resolution. The availability of historical data posed challenges in determining temporal changes over long periods. While remote sensing offers broad coverage and temporal data acquisition, high-resolution data could only be obtained after the 2000s. On the other hand, the use of medium and low spatial resolution images led to decreased accuracy due to the mixed pixel problem (Liu and Trinder 2018; Ling and Foody 2019). To investigate the long temporal period, we employed medium-resolution Landsat satellite images. Nevertheless, based on accuracy assessment, we deemed Landsat images suitable for analyzing substantial changes occurring over long time intervals.

Conclusion

One of the critical consequences of anthropogenic effects on coasts is shoreline changes. Coastal erosion, particularly on sandy beaches, can have severe effects. Therefore, monitoring the shoreline and understanding the underlying causes of these changes is crucial to implement appropriate precautions. This article utilizes remote sensing and GIS technologies to quantitatively assess the effects of a small fishing port on the adjacent beach. Specifically, the study focuses on the erosion caused by the Derekoy Fishing Port, which was constructed in Samsun in 2004 to support the fishing industry—a vital economic activity in the region. The article also examines the impacts of coastal protection structures built to prevent erosion along the coast.

Following the port's construction, accretion was observed in the western part, while erosion occurred in the eastern part due to the obstruction of coastal sand movement. This erosion led to the degradation of sandy beaches in the 19 Mayis and Atakum districts, resulting in significant coastal deterioration. To mitigate coastal erosion, various coastal protection measures such as groins and offshore breakwaters were implemented starting from 2001. However, these structures unintentionally shifted the erosion further eastward while offering localized control. To prevent new erosions, additional coastal protection structures were subsequently constructed, totaling 40 structures by 2018. In

some areas, rock and stone fortifications were employed to combat coastal erosion. However, the study's numerical analysis revealed that erosion persisted and progressively moved eastward, resulting in the loss of 15.62 hectares of beach area from 1984 to 2021. The investigations further highlighted the environmental and socio-economic issues arising from coastal erosion. The deterioration of coastal aesthetics, pollution, reduced beach areas, and the prominent visibility of coastal protection structures and fortifications pose a significant threat to the region's economy, impacting coastal settlements and tourism. The study's findings provide guidance for future development and emphasize the precarious situation of the beaches in the 19 Mayis and Atakum districts, which face an uncertain future due to severe beach erosion along the Samsun coast.

Consequently, it is imperative to consider coastal erosion when constructing ports on sandy beaches, evaluate potential impacts during the port's design phase, and develop effective mitigation plans and strategies to prevent undesirable consequences. Legislative measures should also be enacted to ensure the implementation of necessary measures. Additionally, regular monitoring of coasts and timely interventions in response to changes are essential. Remote sensing offers significant potential for coastal monitoring, and the availability of free data sources presents valuable opportunities. This study utilized Landsat-5 TM/Landsat-8 OLI multispectral images to analyze shoreline changes over periods ranging from 7 to 37 years between 1984 and 2021. The results demonstrate the suitability of Landsat images for identifying long-term shoreline changes and general trends. However, the resolution of the Landsat images may be insufficient for shorter periods, especially in areas with no significant change. Higher spatial resolution images should be used to ensure adequate accuracy in such cases.

Declarations

Competing interests The authors declare that no competing interests exist.

References

Akpınar K (2019) Investigation of the effects of coastal structures on coastal areas in Samsun and Sinop cities using GIS. MSc Thesis, Ondokuz Mayis University, Turkey (in Turkish with English abstract)

Arveti N, Etikala B, Dash P (2016) Land use/land cover analysis based on various comprehensive geospatial data sets: a case study from Tirupati area, south India. Adv Remote Sens 5(2):73–82. https://doi.org/10.4236/ars.2016.52006

Atkinson PM (2001) Super-resolution target mapping from softclassified remotely sensed imagery. In: Proceeding of the 6th International Conference on Geocomputation. University of Queensland, Brisbane, Australia, 24–26 September 2001

Bakkaloğlu S (2006) A study on offshore breakwaters and a case study in Samsun. MSc Thesis, Karadeniz Technical University, Turkey (in Turkish with English abstract)

Barrett JP (1974) The coefficient of determination—some limitations. Am Stat 28(1):19–20. https://doi.org/10.1080/00031305.1974.10479056

Bergillos RJ, Rodríguez-Delgado C, Millares A, Ortega-Sánchez M, Losada MA (2016) Impact of river regulation on a Mediterranean delta: Assessment of managed versus unmanaged scenarios. Water Resour Res 52(7):5132–5148. https://doi.org/10.1002/2015WR018395

Bhatti SS, Tripathi NK (2014) Built-up area extraction using Landsat 8 OLI imagery. Gisci Remote Sens 51(4):445–467. https://doi.org/10.1080/15481603.2014.939539

Boak EH, Turner IL (2005) Shoreline definition and detection: A review. J Coast Res 21(4):688–703. https://doi.org/10.2112/03-0071.1

Burningham H, Fernandez-Nunez M (2020) Shoreline change analysis. In: Jackson D, Short A (eds) Sandy Beach Morphodynamics. Elsevier, Leiden, pp 439–460. https://doi.org/10.1016/B978-0-08-102927-5.00019-9

Candemir F, Özdemir N (2010) Samsun province land resources and soil problems. Anadolu J Agric Sci 25(3):223–229 (in Turkish with English abstract)

Choung YJ, Jo MH (2016) Shoreline change assessment for various types of coasts using multi-temporal Landsat imagery of the east coast of South Korea. Remote Sens Lett 7(1):91–100. https://doi.org/10.1080/2150704X.2015.1109157

Chu DT, Himori G, Saitoi Y, Bui TV, Aoki SI (2015) Study of beach erosion and evolution of beach profile due to nearshore bar sand dredging. Proc Eng 116:285–292. https://doi.org/10.1016/j.proeng.2015.08.292

Claverie M, Vermote EF, Franch B, Masek JG (2015) Evaluation of the Landsat-5 TM and Landsat-7 ETM+ surface reflectance products. Remote Sens Environ 169:390–403. https://doi.org/10.1016/j.rse.2015.08.030

Coca O, Ricaurte-Villota C (2022) Regional patterns of coastal erosion and sedimentation derived from spatial autocorrelation analysis: pacific and Colombian Caribbean. Coasts 2(3):125–151. https://doi.org/10.3390/coasts2030008

Das SK, Sajan B, Ojha C, Soren S (2021) Shoreline change behavior study of Jambudwip island of Indian Sundarban using DSAS model. Egypt J Remote Sens Space Sci 24(3):961–970. https://doi.org/10.1016/j.ejrs.2021.09.004

Daud S, Milow P, Zakaria RM (2021) Analysis of shoreline change trends and adaptation of Selangor Coastline, using Landsat satellite data. J Indian Soc Remote Sens 49(8):1869–1878. https://doi.org/10.1007/s12524-020-01218-0

Deepika B, Avinash K, Jayappa KS (2014) Shoreline change rate estimation and its forecast: remote sensing, geographical information

system and statistics-based approach. Int J Environ Sci Technol 11(2):395–416. https://doi.org/10.1007/s13762-013-0196-1

Dereli MA, Tercan E (2020) Assessment of shoreline changes using historical satellite images and geospatial analysis along the Lake Salda in Turkey. Earth Sci Inform 13(3):709–718. https://doi.org/10.1007/s12145-020-00460-x

Dolan R, Hayden BP, May P, May S (1980) The reliability of shoreline change measurements from aerial photographs. Shore Beach 48(4):22–29

Dugan JE, Airoldi L, Chapman MG, Walker SJ, Schlacher T (2011) Estuarine and coastal structures: environmental effects, a focus on shore and nearshore structures. In: Wolanski E, McLusky DS (eds) Treatise on estuarine and coastal science. Academic Press, Waltham, (8) pp 17–41. https://doi.org/10.1016/B978-0-12-374711-2.00802-0

Elfadaly A, Abutaleb K, Naguib DM, Lasaponara R (2022) Detecting the environmental risk on the archaeological sites using satellite imagery in Basilicata Region, Italy. Egypt J Remote Sens Space Sci 25(1):181–193. https://doi.org/10.1016/j.ejrs.2022.01.007

Evans JD (1996) Straightforward Statistics for the Behavioral Sciences. Brooks/Cole Publishing Company, Pacific Grove

Ghorai D, Mahapatra M (2020) Extracting shoreline from satellite imagery for GIS analysis. Remote Sens Earth Syst Sci 3(1):13–22. https://doi.org/10.1007/s41976-019-00030-w

Gonçalves RM, Saleem A, Queiroz HA, Awange JL (2019) A fuzzy model integrating shoreline changes, NDVI and settlement influences for coastal zone human impact classification. Appl Geogr 113:102093. https://doi.org/10.1016/j.apgeog.2019.102093

Görmüş KS, Kutoğlu ŞH, Şeker DZ, Özölçer İH, Oruç M, Aksoy B (2014) Temporal analysis of coastal erosion in Turkey: a case study Karasu coastal region. J Coastal Conserv 18(4):399–414. https://doi.org/10.1007/s11852-014-0325-0

Güner Ö (2019) Anthropomorphological Structures and Environmental Effects in Atakum (Samsun). East Geog Rev 24(42):67–78 (in Turkish with English abstract)

Himmelstoss EA, Henderson RE, Kratzmann MG, Farris AS (2018) Digital Shoreline Analysis System (DSAS) version 5.0 user guide: U.S. Geological Survey Open-File Report 2018–1179. https://doi.org/10.3133/ofr20181179

Hoang Thi Thu H, Dang Kinh B, Van Rompaey A (2022) Comprehensive assessment of coastal tourism potential in Vietnam. Vietnam J Earth Sci 44(4):1–23. https://doi.org/10.15625/2615-9783/17374

Kavurmacı M, Ekercin S, Altaş L, Kurmaç Y (2013) Use of EO-1 Advanced Land Imager (ALI) multispectral image data and real-time field sampling for water quality mapping in the Hirfanlı Dam Lake. Turkey Environ Sci Pollut Res 20(8):5416–5424. https://doi.org/10.1007/s11356-013-1553-9

Kudale MD (2010) Impact of port development on the coastline and the need for protection. Indian J Geo-Mar Sci 39(4):597–604

Kumar A, Narayana AC, Jayappa KS (2010) Shoreline changes and morphology of spits along southern Karnataka, west coast of India: A remote sensing and statistics-based approach. Geomorphology 120(3–4):133–152. https://doi.org/10.1016/j.geomorph.2010.02.023

Kusimi JM, Dika JL (2012) Sea erosion at Ada Foah: assessment of impacts and proposed mitigation measures. Nat Hazards 64(2):983–997. https://doi.org/10.1007/s11069-012-0216-3

Li L, Chen Y, Xuc T, Liub R, Shi K, Huang C (2015) Super resolution mapping of wetland inundation from remote sensing imagery based on integration of back-propagation neural network and genetic algorithm. Remote Sens Environ 164:142–154. https://doi.org/10.1016/j.rse.2015.04.009

Ling F, Foody GM (2019) Super-resolution land cover mapping by deep learning. Remote Sens Lett 10(6):598–606. https://doi.org/10.1080/2150704X.2019.1587196

Liu Q, Trinder JC (2018) Sub-pixel technique for time series analysis of shoreline changes based on multispectral satellite imagery. In: Marghany M (ed) advanced remote sensing technology for synthetic aperture radar applications, tsunami disasters, and infrastructure. IntechOpen. https://doi.org/10.5772/intechopen.81789

Luo X, Tong X, Qian Z, Pan H, Liu S (2019) Detecting urban ecological land-cover structure using remotely sensed imagery: A multi-area study focusing on metropolitan inner cities. Int J Appl Earth Obs Geoinf 75:106–117. https://doi.org/10.1016/j.jag.2018.10.014

Maiti S, Bhattacharya AK (2009) Shoreline change analysis and its application to prediction: A remote sensing and statistics based approach. Mar Geol 257(1–4):11–23. https://doi.org/10.1016/j.margeo.2008.10.006

Malarvizhi K, Kumar SV, Porchelvan P (2016) Use of high resolution Google Earth satellite imagery in landuse map preparation for urban related applications. Proc Technol 24:1835–1842. https://doi.org/10.1016/j.protcy.2016.05.231

Martínez C, Grez PW, Martín RA, Acuña CE, Torres I, Contreras-López M (2022) Coastal erosion in sandy beaches along a tectonically active coast: The Chile study case. Prog Phys Geogr: Earth Environ 46(2):250–271. https://doi.org/10.1177/03091333211057194

McAllister E, Payo A, Novellino A, Dolphin T, Medina-Lopez E (2022) Multispectral satellite imagery and machine learning for the extraction of shoreline indicators. Coast Eng 174:104102. https://doi.org/10.1016/j.coastaleng.2022.104102

McFeeters SK (1996) The use of the normalized difference water index (NDWI) in the delineation of open water features. Int J Remote Sens 17(7):1425–1432. https://doi.org/10.1080/01431169608948714

Nandi S, Ghosh M, Kundu A, Dutta D, Baksi M (2016) Shoreline shifting and its prediction using remote sensing and GIS techniques: a case study of Sagar Island, West Bengal (India). J Coastal Conserv 20:61–80. https://doi.org/10.1007/s11852-015-0418-4

OSPAR Commission (2009) Assessment of the impact of coastal defence structures. Technical Report, OSPAR Commission Biodiversity Series, London, Publication Number 435/2009

Ouma YO, Tateishi R (2006) A water index for rapid mapping of shoreline changes of five East African Rift Valley lakes: an empirical analysis using Landsat TM and ETM+ data. Int J Remote Sens 27(15):3153–3181. https://doi.org/10.1080/01431160500309934

Özhan E (2002) Coastal erosion management in the mediterranean: an overview. PAP-4/CE/02/PP.1, Priority Actions Programme, Regional Activity Centre, Ankara/Split, Turkey

Ozturk D (2017) Modelling spatial changes in coastal areas of Samsun (Turkey) using a cellular automata-markov chain method. Teh Vjesn 24(1):99–107. https://doi.org/10.17559/TV-20141110125014

Ozturk D, Sesli FA (2015) Shoreline change analysis of the Kizilirmak Lagoon Series. Ocean Coast Manag 118:290–308. https://doi.org/10.1016/j.ocecoaman.2015.03.009

Ozturk D, Beyazit I, Kilic F (2015) Spatiotemporal analysis of shoreline changes of the Kizilirmak Delta. J Coast Res 31(6):1389–1402. https://doi.org/10.2112/JCOASTRES-D-14-00159.1

Pajak MJ, Leatherman S (2002) The high water line as shoreline indicator. J Coast Res 18(2):329–337

Piovan SE (2020) The geohistorical approach: methods and applications. Springer, Cham

Pollard JA, Spencer T, Brooks SM (2019) The interactive relationship between coastal erosion and flood risk. Prog Phys Geogr: Earth Environ 43(4):574–585. https://doi.org/10.1177/0309133318794498

Prasetya G (2006) The role of coastal forests and trees in protecting against coastal erosion. In: Braatz S, Fortuna S, Broadhead J, Leslie R (eds) Coastal protection in the aftermath of the Indian

Ocean tsunami: What role for forests and trees? Proceedings of the Regional Technical Workshop, Khao Lak

Qi F, Wang Y (2014) A new calculation method for shape coefficient of residential building using Google Earth. Energy Build 76:72–80. https://doi.org/10.1016/j.enbuild.2014.02.058

Samsun Chamber of Commerce and Industry (2017) Samsun-Economic Report. Technical Report, Samsun, Turkey, Publication Number 2017/1 (in Turkish)

Scollar I, Palmer R (2008) Using google earth imagery. AARG News 37:15–21

Singh S, Bhat JA, Shah S, Pala NA (2021) Coastal resource management and tourism development in Fiji Islands: a conservation challenge. Environ Dev Sustain 23(3):3009–3027. https://doi.org/10.1007/s10668-020-00764-4

Sowmya K, Sri MD, Bhaskar AS, Jayappa KS (2019) Long-term coastal erosion assessment along the coast of Karnataka, west coast of India. Int J Sediment Res 34(4):335–344. https://doi.org/10.1016/j.ijsrc.2018.12.007

Sunder S, Ramsankaran RAAJ, Ramakrishnan B (2017) Inter-comparison of remote sensing sensing-based shoreline mapping techniques at different coastal stretches of India. Environ Monit Assess 189(6):1–13. https://doi.org/10.1007/s10661-017-5996-1

Suresh M, Jain K (2018) Subpixel level mapping of remotely sensed image using colorimetry. Egypt J Remote Sens Space Sci 21(1):65–72. https://doi.org/10.1016/j.ejrs.2017.02.004

Svatonova H (2016) Analysis of visual interpretation of satellite data. In: The international archives of the photogrammetry, remote sensing and spatial information sciences. Volume XLI-B2, 2016 XXIII ISPRS Congress, Prague

TGDM (Turkish General Directorate of Meteorology) (2022) Official statistics. www.mgm.gov.tr/veridegerlendirme/il-ve-ilceler-istatistik.aspx?m=SAMSUN. Accessed 10 May 2022

Tilahun A, Teferie B (2015) Accuracy assessment of land use land cover classification using Google Earth. Am J Environ Prot 4(4):193–198. https://doi.org/10.11648/j.ajep.20150404.14

TMAF (Turkish Ministry of Agriculture and Forestry) (2022) Fishery coastal structures inventory. https://www.tarimorman.gov.tr/BSGM/Menu/32/Bilgi-Dokumanlari. Accessed 12 Aug 2022

TMEUCC (Turkish Ministry of Environment, Urbanization and Climate Change) (2012) Samsun integrated coastal areas management and planning project-spatial strategy plan. Mekansal Planlama Genel Müdürlüğü, Ankara

TMEUCC (Turkish Ministry of Environment, Urbanization and Climate Change) (2022) The importance of coastal areas. https://mpgm.csb.gov.tr/kiyi-alanlarinin-onemi-i-84350. Accessed 10 Sept 2022

Toure S, Diop O, Kpalma K, Maiga AS (2019) Shoreline detection using optical remote sensing: a review. ISPRS Int J Geo-Inf 8(2):75. https://doi.org/10.3390/ijgi8020075

TSI (Turkish Statistical Institute) (2021) Population and demographics. https://data.tuik.gov.tr/Kategori/GetKategori?p=Nufus-ve-Demografi-109. Accessed 16 Sept 2022

Tsoukala VK, Katsardi V, Hadjibiros K, Moutzouris CI (2015) Beach erosion and consequential impacts due to the presence of harbours in sandy beaches in Greece and Cyprus. Environ Processes 2(1):55–71. https://doi.org/10.1007/s40710-015-0096-0

USGS (U.S. Geological Survey) (2022a) Earth explorer. https://earthexplorer.usgs.gov/. Accessed 7 Feb 2022

USGS (U.S. Geological Survey) (2022b) Landsat collection 2 level-2 science products. https://www.usgs.gov/landsat-missions/landsat-collection-2-level-2-science-products. Accessed 12 Sept 2022

USGS (U.S. Geological Survey) (2022c) Landsat collection 1 vs. collection 2 summary. https://d9-wret.s3.us-west-2.amazonaws.com/assets/palladium/production/s3fs-public/atoms/files/Landsat-C1vsC2-2021-0430-LMWS.pdf. Accessed 14 Oct 2022

Van Rijn LC (2011) Coastal erosion and control. Ocean Coast Manag 54(12):867–887. https://doi.org/10.1016/j.ocecoaman.2011.05.004

Vermote E, Justice C, Claverie M, Franch B (2016) Preliminary analysis of the performance of the Landsat 8/OLI land surface reflectance product. Remote Sens Environ 185:46–56. https://doi.org/10.1016/j.rse.2016.04.008

Weerasingha WADB, Ratnayake AS (2022) Coastal landform changes on the east coast of Sri Lanka using remote sensing and geographic information system (GIS) techniques. Remote Sens Appl: Soc Environ 26:100763. https://doi.org/10.1016/j.rsase.2022.100763

Wiles E, Loureiro C, Cawthra H (2022) Shoreline variability and coastal vulnerability: Mossel Bay. South Africa Estuar Coast Shelf Sci 268:107789. https://doi.org/10.1016/j.ecss.2022.107789

Xu H (2006) Modification of normalised difference water index (NDWI) to enhance open water features in remotely sensed imagery. Int J Remote Sens 27(14):3025–3033. https://doi.org/10.1080/01431160600589179

Yu K, Hu C, Muller-Karger FE, Lu D, Soto I (2011) Shoreline changes in west-central Florida between 1987 and 2008 from Landsat observations. Int J Remote Sens 32(23):8299–8313. https://doi.org/10.1080/01431161.2010.535045

Yüksek Ö (2008) Investigation of erosion on the west coast of Samsun. In: Samsun City Symposium Proceedings Book. Union of Chambers of Turkish Engineers and Architects - Samsun Provincial Coordination Board, Samsun, Turkey, 27–29 November 2008, pp 213–217 (in Turkish)